On Study of Air/Space-borne Dual-Wavelength Radar for Estimates of Rain Profiles

Liang Liao
Goddard Earth Sciences & Technology Center/Caelum, Greenbelt, MD 20771

Robert Meneghini
Code 975, NASA/GSFC, Greenbelt, MD 20771

Submitted to
A Special Issue of *"Advances in Atmospheric Sciences"*

December 2004

Corresponding author information:

Dr. Liang Liao
Goddard Earth Science Technology/Caelum Research Corp.
Code 975
NASA/Goddard Space Flight Center
Greenbelt, MD 20771

301-614-5718 (phone)
301-614-5558 (fax)
Email: lliao@neptune.gsfc.nasa.gov

ABSTRACT

In this study, a framework is discussed to apply air/space-borne dual-wavelength radar for the estimation of characteristic parameters of hydrometeors. The focus of our study is on the Global Precipitation Measurements (GPM) precipitation radar, a dual-wavelength radar that operates at Ku (13.8 GHz) and Ka (35 GHz) bands. As the droplet size distributions (DSD) of rain are expressed as the Gamma function, a procedure is described to derive the median volume diameter (D_0) and particle number concentration (N_T) of rain. The correspondences of an important quantity of dual-wavelength radar, defined as deferential frequency ratio (DFR), to the D_0 in the melting region are given as a function of the distance from the 0^0C isotherm. A self-consistent iterative algorithm that shows a promising to account for rain attenuation of radar and infer the DSD without use of surface reference technique (SRT) is examined by applying it to the apparent radar reflectivity profiles simulated from the DSD model and then comparing the estimates with the model (true) results. For light to moderate rain the self-consistent rain profiling approach converges to unique and correct solutions only if the same shape factors of Gamma functions are used both to generate and retrieve the rain profiles, but does not converges to the true solutions if the DSD form is not chosen correctly. To further examine the dual-wavelength techniques, the self-consistent algorithm, along with forward and backward rain profiling algorithms, is then applied to the measurements taken from the 2^{nd} generation Precipitation Radar (PR-2) built by Jet Propulsion Laboratory. It is found that rain profiles estimated from the forward and backward approaches are not sensitive to shape factor of DSD Gamma distribution, but the self-consistent method is.

Key words: rain rate, dual-wavelength radar, rain drop size distribution and GPM

1. INTRODUCTION

Radar has been shown to be one of the most powerful means to measure rainfall rate. Methods that directly relate a radar measurable such as the radar reflectivity factor, Z, to the precipitation rate, R, are widely used to monitor and estimate the storm evolution and intensity in a variety of storms. Many radar applications use a single wavelength at S- or C-band. In these cases the wavelength is much larger than the hydrometeor sizes so that the assumption of Rayleigh scattering is appropriate for the analysis. An abundance of studies and observations have suggested that the drop size distribution (DSD) is well characterized by the Gamma function (Gorgucci et al. 2001, 2002; Bringi et al. 2002), which generally has more than 2 independent parameters. Theoretically a single wavelength radar is unable to account fully for the variability arising from different meteorological conditions. It is therefore not surprising to see the existence of many Z-R relations reported in the literature (see Gunn and Marshall 1958; Smith 1984; Boucher and Wieler 1985; Matrosov 1992).

Dual-wavelength radar has shown promise to improve the accuracy for estimates of microphysical properties of hydrometeors if one or both wavelengths operate in the non-Rayleigh region (Matrosov 1992; Meneghini et al 1992; Liao et al. 1997; Mardiana et al. 2003). A spaceborne radar operating at Ku (13.8 GHz) and Ka (35 GHz) bands has been proposed as one of the core instruments for the Global Precipitation Measurement Mission (GPM) (Iguchi et al. 2002) and will serve as a calibrator for other instruments aboard the GPM satellite in mapping precipitation globally. However, the radar returns suffer from attenuation while propagating through the rain, cloud and mixed-phase precipitation. This attenuation not only complicates the radar retrieval of rain but also affects the accuracy of the algorithms if the attenuation is not properly corrected.

In this study, we focus on dual-wavelength air/space-borne radar techniques and their application to the radar measurements for the estimation of characteristic parameters of hydrometeors. Having described the results of how the dual-wavelength measurements are linked to the DSD parameters, a self-consistent iterative approach for deriving the hydrometeor profile is numerically examined based on the simulation of the GPM spaceborne radar returns. Analysis of the results is also given.

2. FRAMEWORK OF DUAL-WAVELENGTH TECHNIQUES

The effective radar reflectivity factor of the hydrometeors at wavelength λ is given as

$$Z_e = \frac{\lambda^4}{\pi^5 |K_w|^2} \int_0^\infty N(D)\sigma_b(D,\lambda)dD, \tag{1}$$

where N(D) is the particle size distribution and $\sigma_b(D,\lambda)$ the backscattering cross section. K_w, the dielectric factor, is used to designate $(m^2-1)/(m^2+2)$, where m is the complex refractive index of water. By convention, $|K_w|^2$ is taken to be 0.93. While Z_e can be determined from the radar return signal if attenuation is accounted for, $\sigma_b(D,\lambda)$ is directly computed by Mie theory. Finding a solution to the parameters of the N(D) from (1) is an inverse problem that can be solved by use of radar measurements.

The hydrometeor size distributions can be accurately described by the Gamma function. A form of the Gamma size distribution of N(D), used widely in the retrieval of the microphysical properties of hydrometeors, is expressed as

$$N(D) = N_0 D^{\mu} \exp\left[-(3.67+\mu)\frac{D}{D_0}\right], \tag{2}$$

where N_0 is constant, D the particle diameter, D_0 the median volume diameter of the particle and μ the shape factor. The number concentration, N_T, can be expressed in terms of these variables by:

$$N_T = N_0 \Gamma(\mu+1)/G^{\mu+1}, \tag{3}$$

$$G = (3.67+\mu)/D_0, \tag{4}$$

where Γ is the Gamma function. The radar dual-frequency ratio (DFR) in dB, describing the difference of the radar reflectivity at 2 wavelengths, is defined as

$$DFR = 10\log(Z_u / Z_v), \tag{5}$$

where Z_u and Z_v are the radar reflectivity factors at wavelengths of λ_u and λ_v. The DFR is independent of the N_0 as can be inferred from (1), (2) and (5).

Figure 1 shows the results of DFR versus D_0 for the Gamma distribution of rain given by (2) for the case of the GPM radar. At a fixed μ, the D_0 is solely dependent on the DFR over the range where D_0 is great than 1 mm. The one-to-one relation of D_0 and DFR provides a possible means to infer D_0 if the attenuation is corrected for the DFR. However, double roots of D_0 appear for a given DFR when its value is less than 0, with one solution from the lower branch of the DFR-D_0 relation and another from the higher branch. This feature, however, leads to an ambiguity for estimates of D_0. The ambiguity might be lessened if the radar reflectivity is used to aid in the selection of the proper roots. To take a closer look at how the D_0 and N_T are inferred from the dual-wavelength radar measurements, contour plots of D_0 and N_T are shown in Fig. 2 mapped onto the plane of DFR (ordinate) and radar reflectivity at Ku band (abscissa). Note for the case shown, μ=2. The top pannel of Fig. 2 shows the upper branches of the DFR-D_0 relation while the bottom pannel displays the results of the lower branches. The thick dashed lines are the values of DFR that separate the upper and lower branches. Equivalently this DFR corresponds to

D_0 of 0.91 mm. In the upper region (top), the D_0 nicely responds to the DFR in the sense that the DFR has a good dynamic range (~10 dB) as D_0 varies from 0.91 to 2.5 mm. The N_T, which can be obtained from D_0 and either of the radar reflectivities at Ku or Ka bands, seems to be sensitive to the radar reflectivity and DFR or D_0 as demonstrated by the dense equal-space contour plots of N_T. This tends to more apparent as the N_T increases. For the region where DFR is less than 0 (bottom panel of Fig.2), the lower branches are given in blue lines. For reference, the upper branches (red) are also superimposed on the plot. The existence of 2 solutions (from blue and red lines) of D_0 for a DFR whose value is less than 0, poses a problem as to how to choose the solution. A lack of knowledge in identifying the solution eventually leads to uncertainties or errors in the estimates of D_0. It is clearly shown in Fig.2 that using the data of the reflectivity at Ku band enables us to narrow the selection of D_0. For example, for a DFR in the range from –4 to 0 dB and the Ku-band radar reflectivity less than 10 dBZ, a solution from the lower branch should be chosen. For the same range of DFR but with the radar reflectivity greater than 20 dBZ, the upper branch should be selected for determining D_0. The intersection of the lower (blue) and upper (red) branches is the area where it is not possible to find a unique solution. This is identified as one of the sources of error in the dual-wavelenght method. The results of Fig.2 illustrate how the DSD parameters are associated with the dual-wavelength radar measurables. This serves as a basis for the retrieval of the raindrop size distribution.

In the melting region, in which a radar bright band is often observed, the DFR-D_0 relation is much more complex than in the rain. To briefly describe the DFR-D_0 relation in the melting layer, we present an example, as shown in Fig.3, of DFR at Ku and Ka bands as a function of D_0 and distance from the 0°C isotherm. The melting layer model used for the computation has been described by Yokoyama and Tanaka (1984) in which no aggregation and drop breakup are

included. The stratified-sphere scattering model is utilized for computations of the radar scattering intensities from the melting hydrometeors whose fractional water contents are prescribed as a function of radius (Liao and Meneghini, 2004). At the 0°C level where only snowflakes are present, the DFR is in one-to-one relation with D_0. Below the 0°C, the melting starts and proceeds until all the hydrometeors become raindrops. The DFR-D_0 relations with respect to these stages are clearly displayed in Fig.3. For distances between 0 and 1 km where melting takes place, double values of D_0 occur at small values of DFR. For a fixed distance from the 0°C isotherm, the minimum D_0, which occurs at the point where the lower and upper branches merge, is a small value at the early stage of melting and then gradually increases as the rain region is approached. The DFR reaches its maximum value in the rain (about 1 km) and maintains this value thereafter. Note that the D_0 used here is defined as the melted medium volume diameter. Implementation of the DFR-D_0 relations in the melting layer is a greater challenge to the radar retrievals than rain because of their complex nature of the scattering. Studies of the scattering properties of the melting layer and the use of these results in the precipitation retrieval algorithms are ongoing.

3. DUAL-WAVELENGTH ALGORITHMS

The Ku and Ka band radars are subject to attenuation while traveling in the rain. The attenuation needs to be corrected at both wavelengths before using the procedures described in section 2 for the retrieval of the DSD and rain profiles. Several dual-wavelength profiling algorithms have been described by Meneghini et al. (1992). They are generally classified as the forward and backward approaches for solving the radar integral equations. For the forward approach, the gate-by-gate retrievals are conducted along the radar-transmitted direction while

the backward is done in reverse order from the surface upward. For the airborne or spaceborne radar, the forward approach starts at the storm top. The advantage of the forward approach is that there is no need of any constraint. The attenuation at a gate is corrected based on the estimated DSD of previous gates. This procedure, however, is unstable for moderate and high rain attenuation, and can easily diverge as it proceeds deep into the storm. In addition to this, the method encounters difficulties that arise from the melting layer model or the assumed magnitude and vertical distribution of cloud liquid water. Therefore, it is of limited utility for practical dual-wavelength applications. The backward approach, starting at the surface, needs the constraints of the path integrated attenuation (PIA), which are generally obtained by the surface reference technique (SRT) (see Meneghini et al., 2000) or the standard dual-wavelength method (STD) if the SRT is not available. Estimation of PIA by the SRT is based on the fact that the difference of radar normalized surface cross section between rain and rain-free areas are primarily attributed to path attenuation. The standard dual-wavelength method estimates the PIA under the assumption that the difference in the apparent radar reflectivities at two wavelengths results from the difference in their respective PIAs. This is an approximation, which is true only if Rayleigh scattering holds for both wavelengths at the end gates of the path over which the PIA is estimated. In contrast to the forward approach, the backward procedures are stable and immune to problems caused by the presence of cloud water and by uncertainties of modeling bright band. They, however, suffer from errors as a result of inaccurate estimates of PIA, such as intrinsic surface changes between the regions with and without rain for the SRT. For the standard dual-wavelength method, errors arise when non-Rayleigh scattering occurs at the beginning or end range gates of the path.

A self-consistent backward iterative method has recently been devised and studied (Mardiana et al. 2003). The basic principle is to seek the DSD that can not only reproduce the radar reflectivity profiles at two wavelengths but also the path attenuations that are used for the constraints prior to deriving the DSD profile. The procedure can be mathematically described as follows.

For simplicity but without losing generality, we consider a rain profile that consists of n equal-range gates. The range gates, r_i, i=1, 2, …, n, are counted starting from the storm top (r_1) to the surface (r_n). The D_0, N_T and specific attenuation (k in dB/km) can be expressed as

$$\begin{aligned} D_0(r_i) &= p(DFR(r_i)) \\ N_T(r_i) &= q(D_0(r_i), Z_e^{(1)}(r_i)) \\ k^{(1)}(r_i) &= u(D_0(r_i), N_T(r_i)) \\ k^{(2)}(r_i) &= v(D_0(r_i), N_T(r_i)) \end{aligned}, \tag{6}$$

where p, q, u and v are the known functions, and Z_e is the true reflectivity. The superscripts (1) and (2) represent the 1st and 2nd frequencies of the dual-wavelength radar. Like the backward approaches described previously, the self-consistent backward iterative approach needs PIA constraints before inferring the DSD profile. The procedure begins with initial guesses of the PIA at both frequencies so that the true radar reflectivity at the surface is calculated from the measured reflectivity factor and the PIA by

$$\begin{aligned} Z_e^{(f)}(r_n) &= Z_m^{(f)}(r_n) + PIA^{(f)} \\ f &= 1,2 \end{aligned}, \tag{7}$$

where Z_m stands for the apparent or measured reflectivity. Using (7), the $D_0(r_n)$, $N_T(r_n)$, $k^{(1)}(r_n)$ and $k^{(2)}(r_n)$ are derived using (6). In a similar way, we proceed to (n-1)th gate and the path attenuation, A, of radar to the (n-1)th gate is obtained by subtracting the attenuation at nth gate from the PIA, i.e., $A^{(f)}(r_{n-1}) = PIA^{(f)} - 2k^{(f)}(r_n)\Delta r$, f=1,2, where $\Delta r = r_n - r_{n-1}$ is the radar range

resolution. A factor of 2 represents the 2-way attenuation. Following the same procedure, we have the results at the ith gate as follows,

$$Z_e^{(f)}(r_i) = Z_m^{(f)}(r_i) + \left[PIA^{(f)} - 2\sum_{j=i+1}^{n} k^{(f)}(r_j)\Delta r \right]. \quad f = 1,2 \tag{8}$$

The D_0, N_T and k are then obtained at the ith gate from (6). Continuing this procedure to the storm top, the DSD profile is generated, and subsequently the PIA is computed. The newly derived results of the PIA are compared with those used as the constraints before starting the estimation process. The differences between the current and previous PIA are used to make adjustments to the previous PIAs, which are subsequently used as new constraints for the next iteration. As a matter of fact, the adjusted PIAs are the result of the path attenuations calculated from the DSD profile, which are

$$PIA^{(f)} = 2\sum_{i=1}^{n} k^{(f)}(r_i)\Delta r \quad f = 1,2 \tag{9}$$

The iterative procedure is considered to converge if the difference between the PIA derived at the current and previous steps are smaller than a predefined value.

To check the convergence of the iterative procedure and uniqueness of solution of the DSD profile, we conduct simulations in which the DSD profiles are assumed to be realizations of the Gamma distribution. With the DSD profiles, we are able to generate the dual-wavelength radar profiles. Shown in the left-top panel of Fig.5 is an example of Ku (red) and Ka (blue) band radar profiles. The solid and dashed lines are the true and apparent radar reflectivity. The rain height is 5 km. A vertically inhomogeneous rain profile is considered with the D_0 linearly varying from 1.2 mm at the storm top to 1.7 mm at the surface and the corresponding N_T changing from 400 to 200 m^{-3}. The μ of the Gamma distribution is 2. Consequently, the rain rate linearly increases

from the storm top to the surface, as illustrated in the right-top panel of Fig.5. Using the apparent reflectivity profiles, the iterative procedures described by (6)-(9) are carried out with various initial guesses of the PIAs as μ is selected to 2 (same as what is used to generate the radar profiles). The intermediate results of DSD, rain rate and PIAs at the surface (the nth gate) are plotted in Fig.4 at each step of iteration for the purpose of monitoring their convergence. Different line styles denote the results from different initial values of the PIAs. Of these results, the solid lines are the results when the initial PIAs are set to zero at both frequencies. For other cases, the initial PIAs are taken both as positively and negatively biased from the true PIAs. These can be seen in the right-bottom panel of Fig.4 in which the results of the PIAs at Ku (red) and Ka (blue) bands are displayed. In general, the PIA at Ku band converges much faster than that at Ka band. Overall, all the results demonstrate that the iteration not only converges but converges to the unique solution regardless of the initial PIAs. The slight differences between the retrieved and true values are probably attributable to numerical errors associated with the iterations. The final results of the DSD and rain profiles are compared to the true profiles in Fig.5, where the thick red lines represent the true values. The retrieval results are given by the thin dark lines with the line styles matched to the cases in Fig.4. Because the results converge to nearly the same solution, they are almost indistinguishable in the plots. The derived profiles are in excellent agreement with the true ones. We conclude that when the same DFR-D_0 relations are used both to generate and to retrieve the profiles, the backward iteration converges to the correct solution for light and moderate rain rates irrespective of the initial PIA values used. For relatively high rain rates, however, our simulations show that the iterative approach does not converge.

To check how the convergence of solutions is affected if the different DFR-D_0 relation is used for the retrieval, i.e., μ is taken to a different value from the one used to produce the radar profiles, we repeat the above procedures as μ is set to 4 for the DSD used for the retrieval (while μ of 2 is used to generate the original radar profiles). Figure 6 presents the results of convergence for the D_0, N_T, rain rate and PIAs at the gate near the surface as they are inferred at μ=4. Obviously, all the solutions tend to converge no matter what initial values are used, but they converge to wrong ones. This may lead an error for the retrieval of rain parameters if an incorrect μ is assumed. Further tests (not shown) reveal that appearances of cloud liquid water may also present an error for the retrieval if its attenuation is not accurately corrected. It should be noted that our results reported here should be considered preliminary. Further simulations are needed to account for the melting layer and cloud effects.

4. RAIN RETRIEVAL FROM RADAR MEASUREMENTS

To assess the performances of the dual-wavelength techniques discussed previously for the retrieval of rain profile, we employ the PR-2 airborne Ku and Ka band radar data taken from the measurements during the 4th field campaign of the Convection And Moisture EXperiment (CAMEX-4) in Florida, 2001. A description of the PR-2 radar has been given by Eastwood et al. (2000). Figure 7 displays the PR-2 radar measurements from a storm cell on the 25th of September in 2001, where majority of storm is stratiform rain and only a small portion is convective storm. With the high range resolution of the PR-2 the bright band is clearly define. Because of severe rain attenuation, the surface signals are lost in the Ka-band channel at the place where relatively intensive rain is present (after 00:23:40 UT). The DFR of the Ku and Ka bands are plotted in the third panel from the top of Fig.7, and the surface returned powers are

given in the bottom panel. Due to lack of the data prior to 00:19:40 UT and failure to detect the surface after 00:23:40 UT at Ka band, we confine our retrievals only to the region where the complete measurements of rain profiles and surface are available. This is corresponding to the time between 00:19:39 and 00:23:39 UT, when the stratiform rain is observed. To avoid the uncertainties and difficulties stemming from modeling the bright band, the retrievals are limited to the rain region. Figure 8 shows the estimates of rain rate from the forward (FW) and backward (BW) approaches with use of SRT and STD for the constraint of PIA as well as self-consistent backward (SELF-BW) iterative algorithm. The attenuations of radar signals while traveling in melting layer, snow and cloud (above freezing level) are approximated by the differences between the PIA and the path attenuation in the rain region estimated by the SRT. They are subsequently used to the first gate (top of the rain) for the forward approach to account for the attenuation contributed from the bright band, snow and cloud water. Thus, the rain rates at the first gate from the rain top derived from the FW should match the results obtained from the SRT-BW. The left panels of Fig.8 are the results of the estimated rain rate as μ is assumed to 2 while the right panels are ones as μ is assumed to 6. These results, in general, are in fairly good agreement among the approaches within their convergence regions. For the light rain the FW is able to get the results for the entire profiles but fails to reach the surface for the relatively heavy rain. As expected, the backward approaches are relatively stable and can produce the results for most of storm, so does the self-consistent method. Around 00:21:15 UT the radar echoes are so weak (with a level close to minimum detectable signal) that the noise-induced variation of radar reflectivity impairs the PIA estimations by the STD and the self-consistent method, leading to the gap of their retrievals. For the regions where the SRT-BW fails to produce the results, the surface fluctuations are believed to be a factor. It is interesting to find that rain profiles estimated

from the forward and backward approaches are not sensitive to shape factor of DSD Gamma distribution as indicated by the comparisons between the left and right panels of Fig.8, but the self-consistent method is.

5. SUMMARY

A description of dual-wavelength techniques is given for the retrieval of rain profiles. The results linking the radar measurables to the DSD parameters are computed for the GPM radar that operates at the Ku and Ka bands. The air/space-borne dual-wavelength radar profiling algorithms are discussed, and an iterative backward approach is numerically examined for its validity. We conclude that for light to moderate rain rates the iterative procedure converges to the correct solution if the same DSD parameters (i.e., μ and temperature) are used both to generate and retrieve the radar profiles, but does not converges to the true solutions if the DSD form is not chosen correctly. To make an assessment for the dual-wavelength techniques, the various rain-profiling algorithms are applied to the measurements taken from the PR-2 during CAMEX-4 in 2001. Comparisons of the results show that rain profiles estimated from the forward and backward approaches are not sensitive to shape factor of DSD Gamma distribution, but the self-consistent method is. In our future studies the bright band and cloud water will be included in our simulations to further test the various methods that have been proposed.

ACKNOWLEDGEMENTS

We wish to thank JPL for providing the PR-2 radar data and its processing software.

REFERENCES

Bringi, V., G. Huang, V. Chandrasekar and E. Gorgucci, 2002: A methodology for estimating the parameters of a Gamma raindrop size distribution model from polarimetric radar data: Application to a squall-line event from the TRMM/Brazil campaign. *J. Oceanic and Atmos. Tech.*, **19**, 633-645.

Boucher, R. J., and J. G. Wieler, 1985: Radar determination of snowfall rate and accumulation. *J. Climate Appl. Meteor.*, **24**, 68-73.

Gorgucci, E., G. Scarchilli, V. Chandrasekar and V. Bringi, 2001: Estimation of raindrop size distribution parameters from polarimetric radar measurements. *J. Atmos. Sci.*, **59**, 2373-2384.

Gunn, K. L. S., and J. S. Marshall, 1958: The distribution with size of aggregate snowflakes. *J. Meteor.*,**15**, 452-461.

Iguchi, T., R. Oki, E.A. Smith and Y. Furuhama, 2002: Global Precipitation Measurement program and the development of dual-frequency precipitation radar. *J. Commun. Res. Lab. (Japan)*, **49**, 37-45.

Im, E. et al, 2000: The tropical rainfall measuring mission (TRMM) sensor package. Proceedings of IGARSS'00.

Liao, L., R. Meneghini, T. Iguchi and A. Detwiler, 1997: Estimation of snow parameters from dual-wavelength airborne radar. Preprints 28th Conf. Radar Meteor., American Meteor. Soc., 510-511.

------, and R. Meneghini, 2005: On modeling air/space-borne radar returns in the melting layer. (To be submitted to *IEEE trans. Geosci. Remote Sens.*)

Mardiana, R., T. Iguchi, N. Takahashi, and H. Hanado, 2003: Dual-frequency rain profiling method without the use of surface reference technique. Proceedings of IGARSS'03.

Matrosov, S. Y., 1992: Radar reflectivity in snowfall. *IEEE Trans. Geosci. Remote Sens.*, **30**, 454-461.

Meneghini, R., T. Kozu, H. Kumagai, and W. C. Boncyk, 1992: A study of rain estimation methods from space using dual-wavelength radar measurements at near-nadir incidence over ocean. *J. Atmos. Oceanic Technol.*, **9**, 364-382.

------, T. Iguchi, T. Kozu, L. Liao, K. Okamoto, J. A. Jones, and J. Kwiatkowski, 2000: Use of the surface reference technique for path attenuation estimates from TRMM precipitation radar. *J. Appl. Meteor.*, **39**, 2053-2070.

Yokoyama, Y., and H. Tanaka, 1984:Microphysical process of melting snowflakes detected by two-wavelength radar. *J. Meteor. Soc. Japan*, **62**, 650-666.

Figure Captions:

Fig.1 DFR of Ku and Ka bands versus D_0 of rain at several values of μ.

Fig.2 Multi-parameter plots of D_0 (mm) and N_T (m^{-3}) on the planes of the radar reflectivity at Ku band and DFR. The top panel represents the results of the upper branch of the DFR-D_0 relation while the lower panel gives the results of the lower branch (blue). For reference, the results of the upper branch are also plotted in the lower panel.

Fig.3 The DFR-D_0 relations of the melting layer expressed as a function of the distance below 0°C isotherm for Ku and Ka bands. The computations are made for a snow density of 0.2 g/cm^3 and μ of 2.

Fig.4 Plots of the results of the D_0, N_T, rain rate and PIAs at the surface using the self-consistent backward iterative method in terms of number of iterations. Different line styles represent the results that are derived under different initial values for the PIAs. The straight lines parallel to the abscissa are the true results. In the plot of the PIA (right-bottom panel), the blue lines represent the Ka band results and the red represents the Ku band results. The shape factor μ of Gamma function is 2 for the retrieval, which is the same as the one used for simulations of radar profiles (left-top panel of Fig.5).

Fig.5 The simulated radar reflectivity profiles of Ku (red) and Ka (blue) bands shown in the left-top panel where the solid and dashed lines describe the true and apparent radar reflectivity, respectively, as μ equals to 2. The profiles of D_0, N_T and rain, derived from the iterative

backward procedure, are compared with the true values (thick red lines). The inferred profiles are given by the dark lines with various line styles in correspondence with the initial guesses of the PIAs shown in Fig.4.

Fig.6 Same as Fig.4 but for the case where μ of Gamma function for the retrieved DSD is assumed to 4.

Fig.7 The PR-2 measurements over a rain cell taken on 25 September 2001 in Florida during the CAMEX-4. The surface powers are also plotted (bottom panel) with the upper curve denoting the Ku band and the lower the Ka band.

Fig.8 Estimates of rain rate from the PR-2 measurements shown in Fig.6 by use of forward, backward and self-consistent approaches as μ is assumed to 2 and 6.

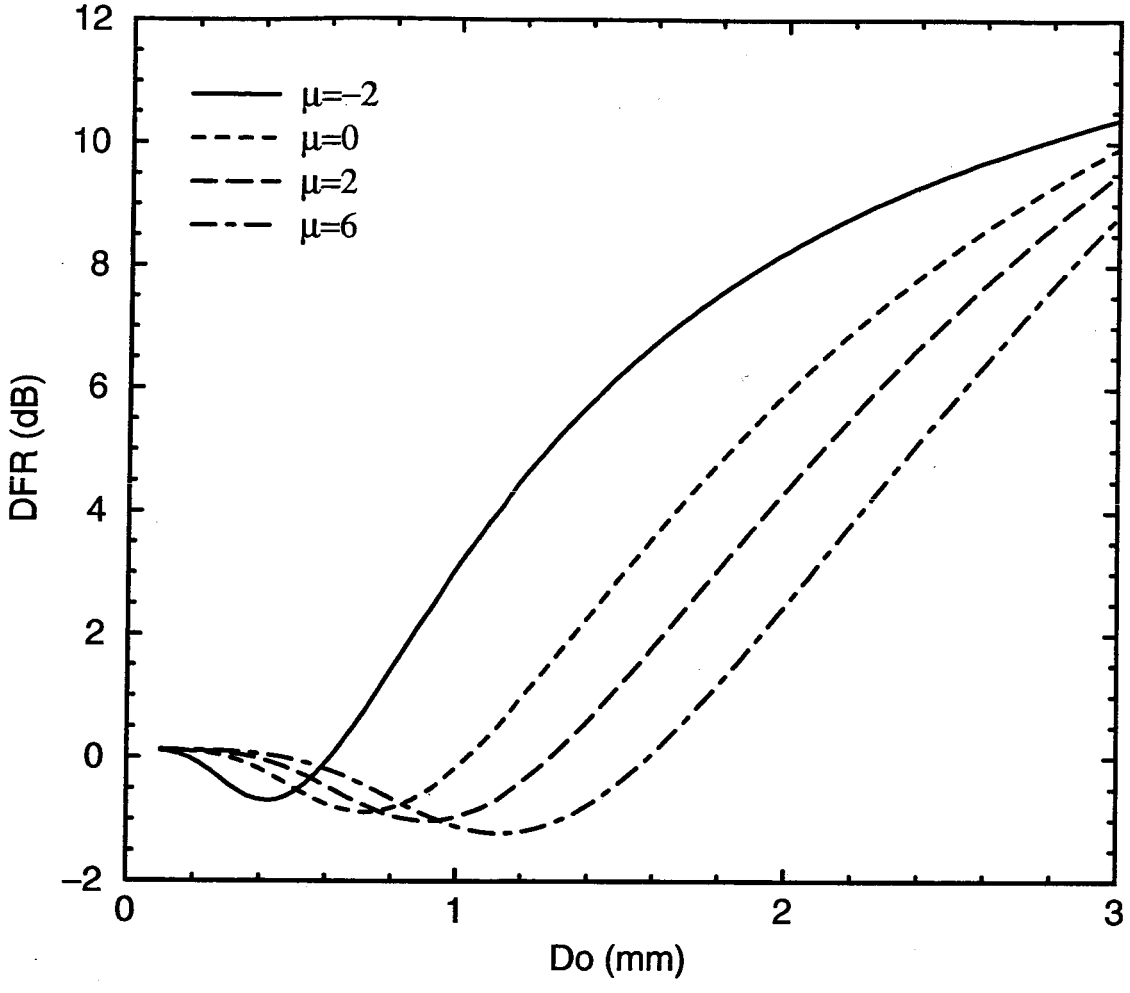

Fig.1 DFR of Ku and Ka bands versus D_0 of rain at several values of μ.

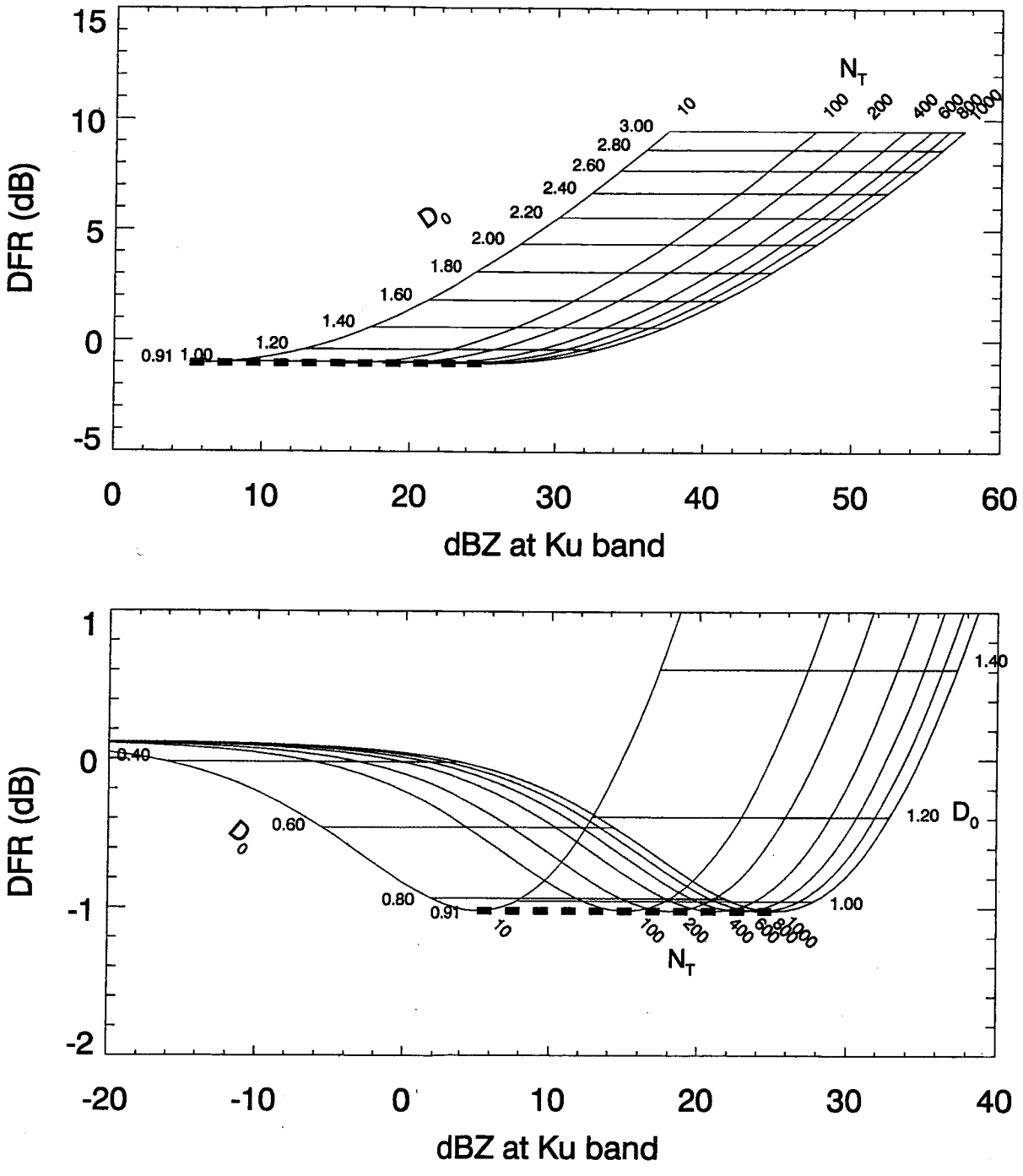

Fig.2 Multi-parameter plots of D_0 (mm) and N_T (m^{-3}) on the planes of the radar reflectivity at Ku band and DFR. The top panel represents the results of the upper branch of the DFR-D_0 relation while the lower panel gives the results of the lower branch (blue). For reference, the results of the upper branch are also plotted in the lower panel.

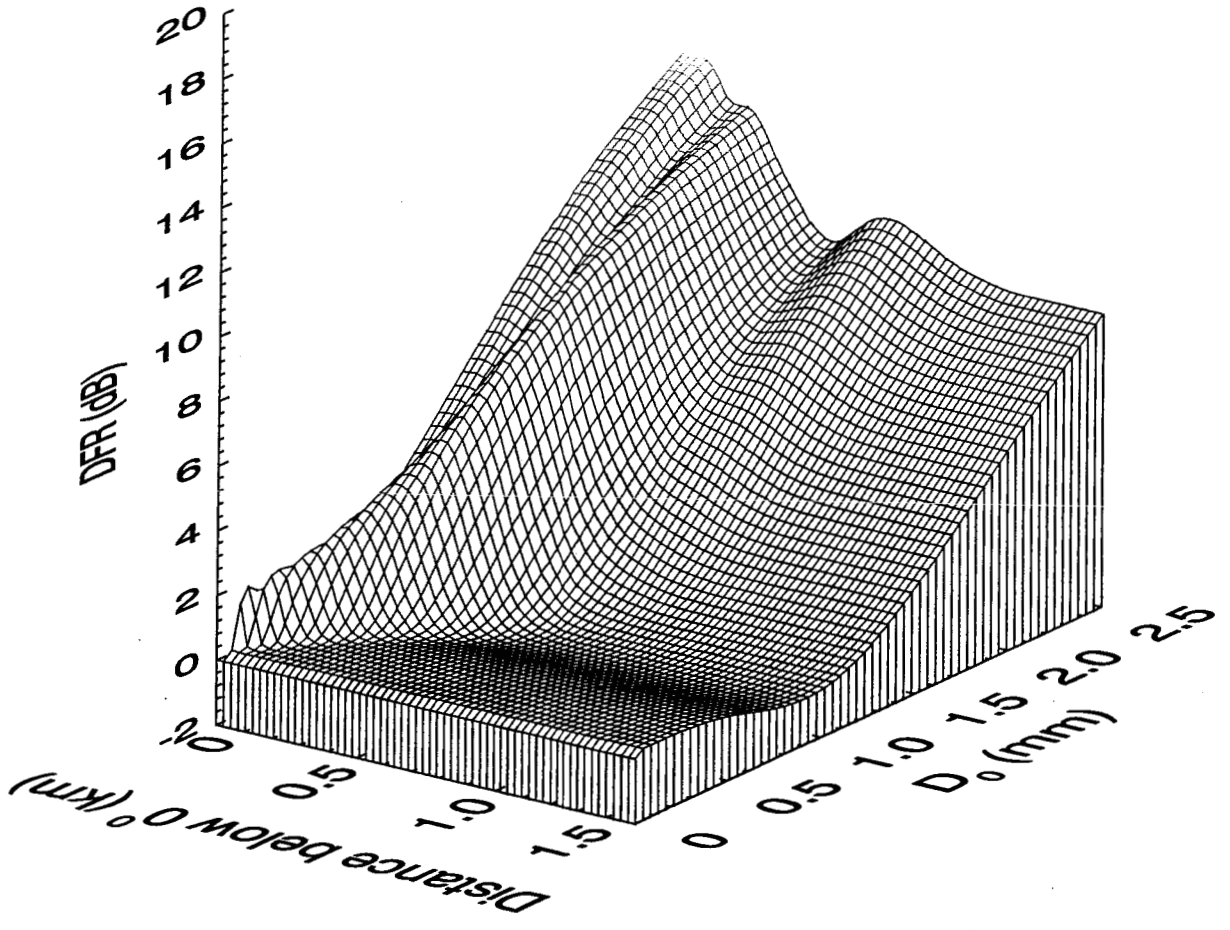

Fig.3 The DFR-D_0 relations of the melting layer expressed as a function of the distance below 0°C isotherm for Ku and Ka bands. The computations are made for a snow density of 0.2 g/cm^3 and μ of 2.

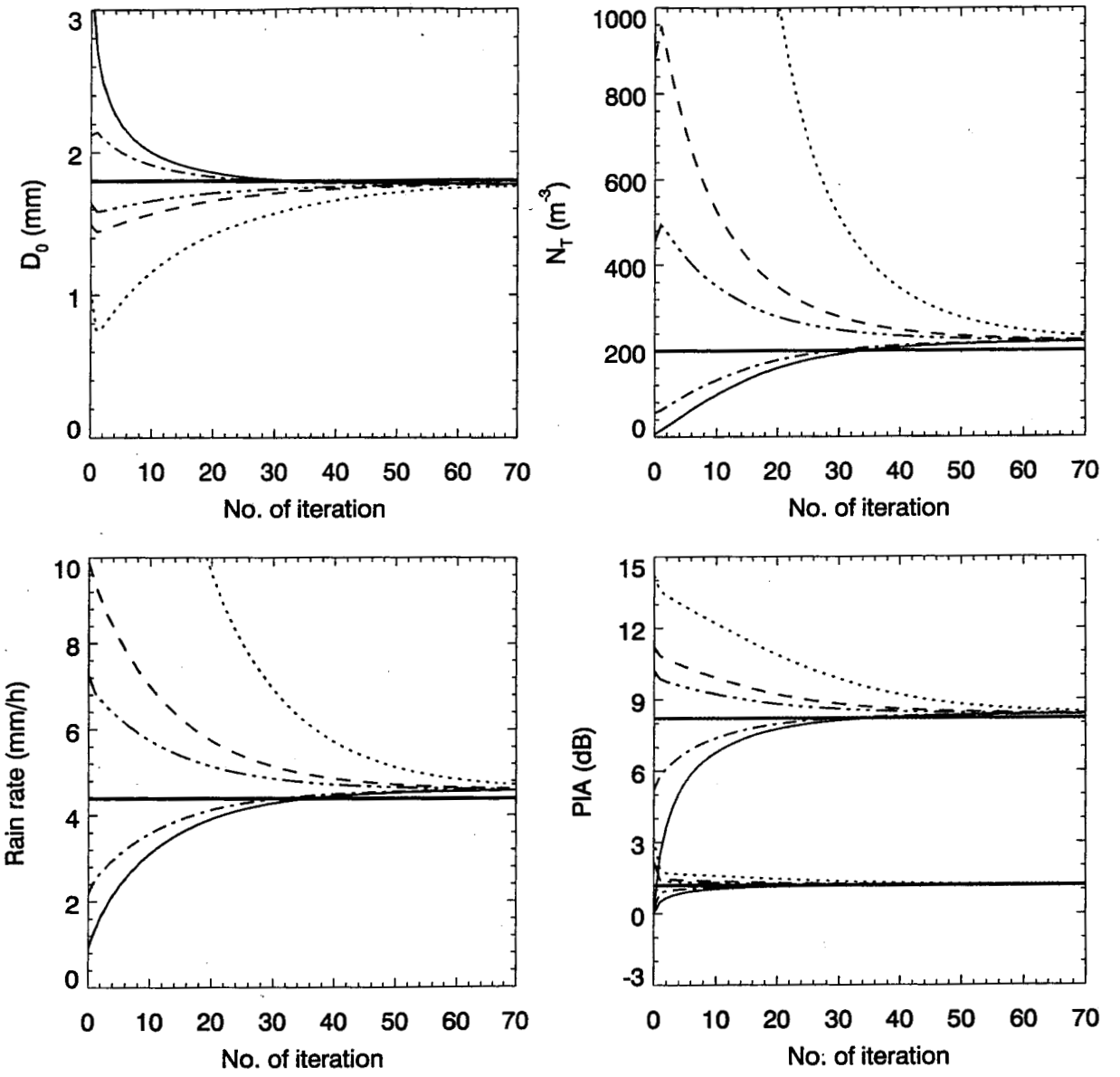

Fig.4 Plots of the results of the D_0, N_T, rain rate and PIAs at the surface using the self-consistent backward iterative method in terms of number of iterations. Different line styles represent the results that are derived under different initial values for the PIAs. The straight lines parallel to the abscissa are the true results. In the plot of the PIA (right-bottom panel), the blue lines represent the Ka band results and the red represents the Ku band results. The shape factor μ of Gamma function is 2 for the retrieval, which is the same as the one used for simulations of radar profiles (left-top panel of Fig.5).

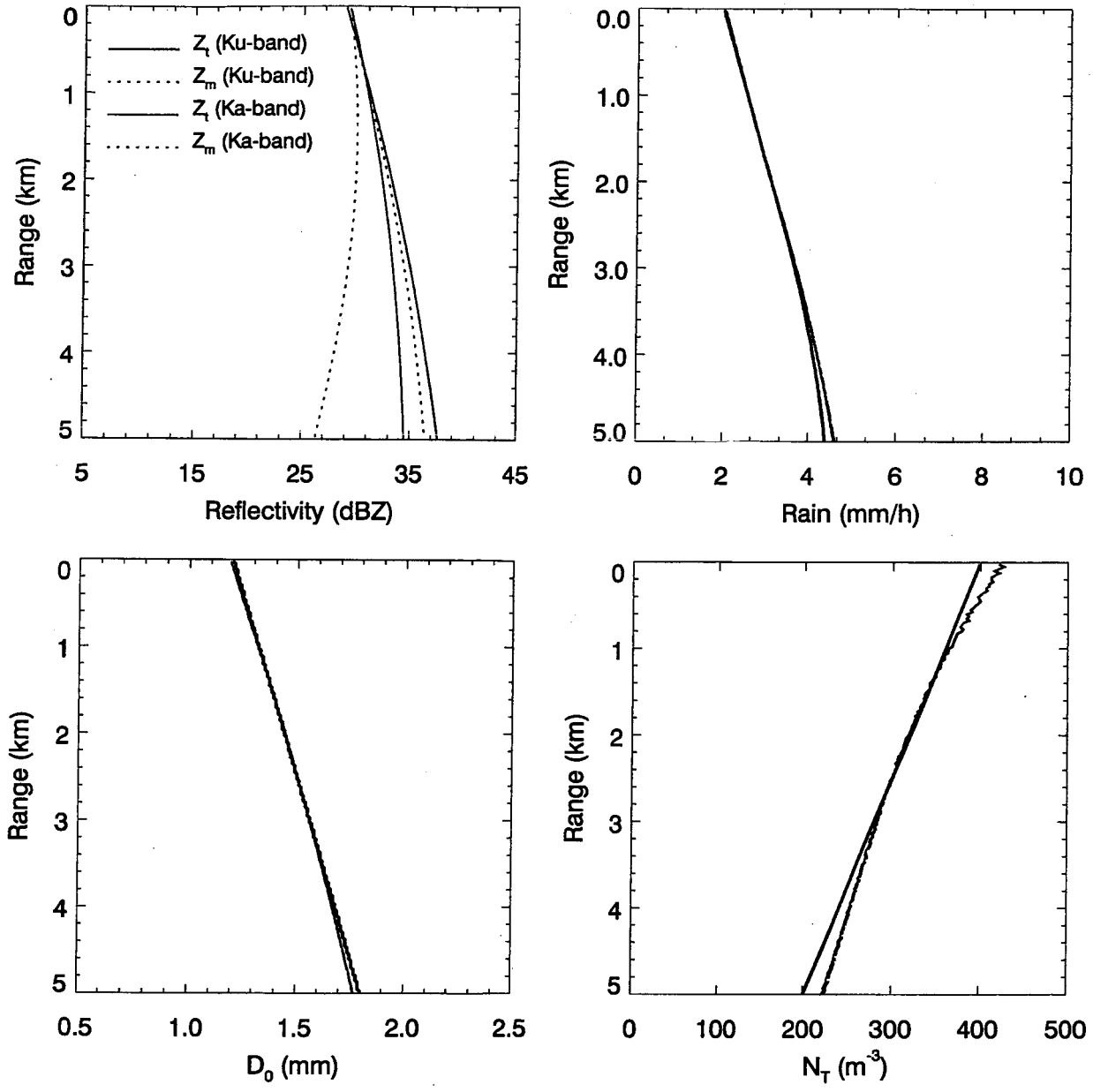

Fig.5 The simulated radar reflectivity profiles of Ku (red) and Ka (blue) bands shown in the left-top panel where the solid and dashed lines describe the true and apparent radar reflectivity, respectively, as μ equals to 2. The profiles of D_0, N_T and rain, derived from the iterative backward procedure, are compared with the true values (thick red lines). The inferred profiles are given by the dark lines with various line styles in correspondence with the initial guesses of the PIAs shown in Fig.4.

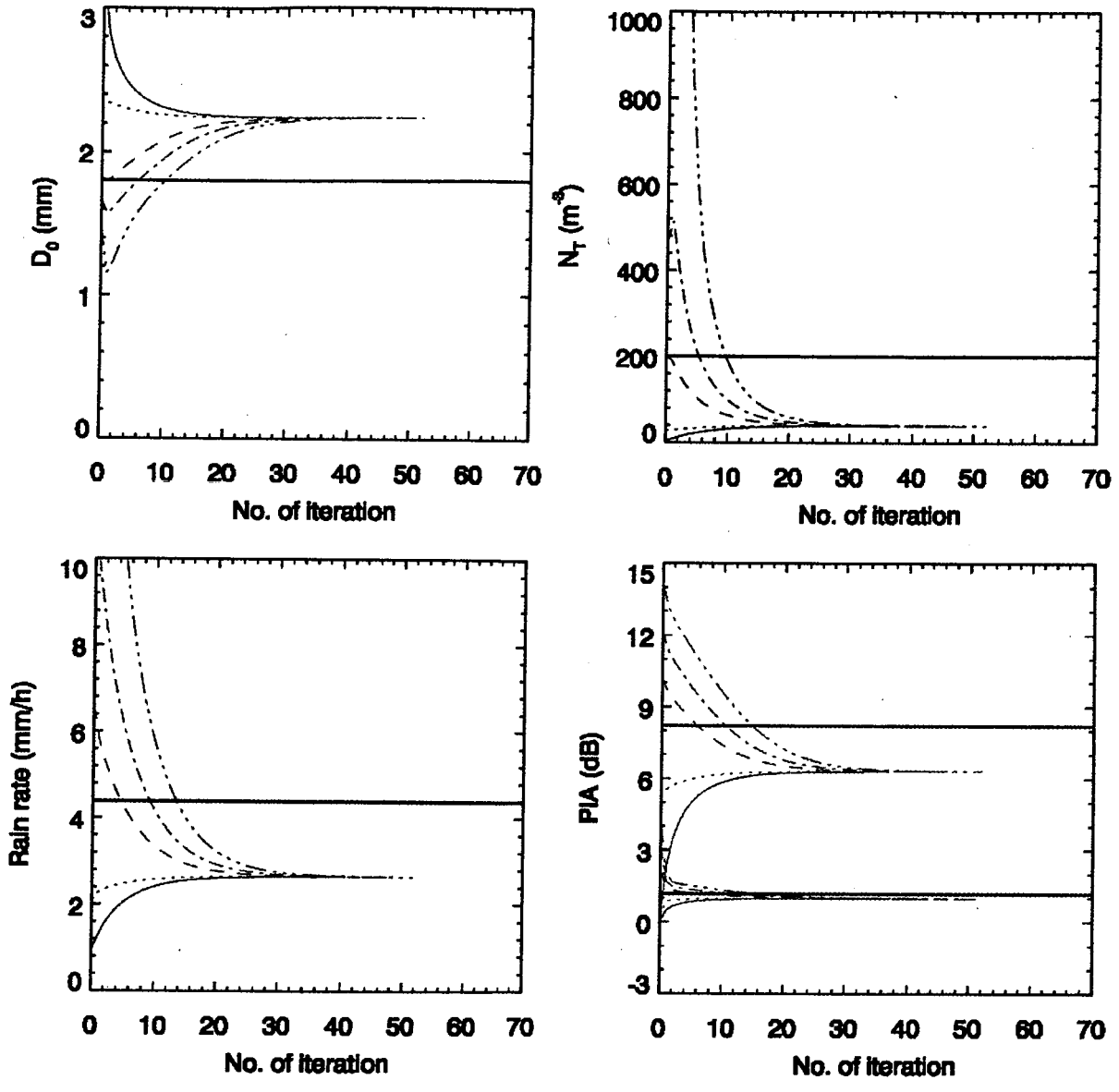

Fig.6 Same as Fig.4 but for the case where μ of Gamma function for the retrieved DSD is assumed to 4.

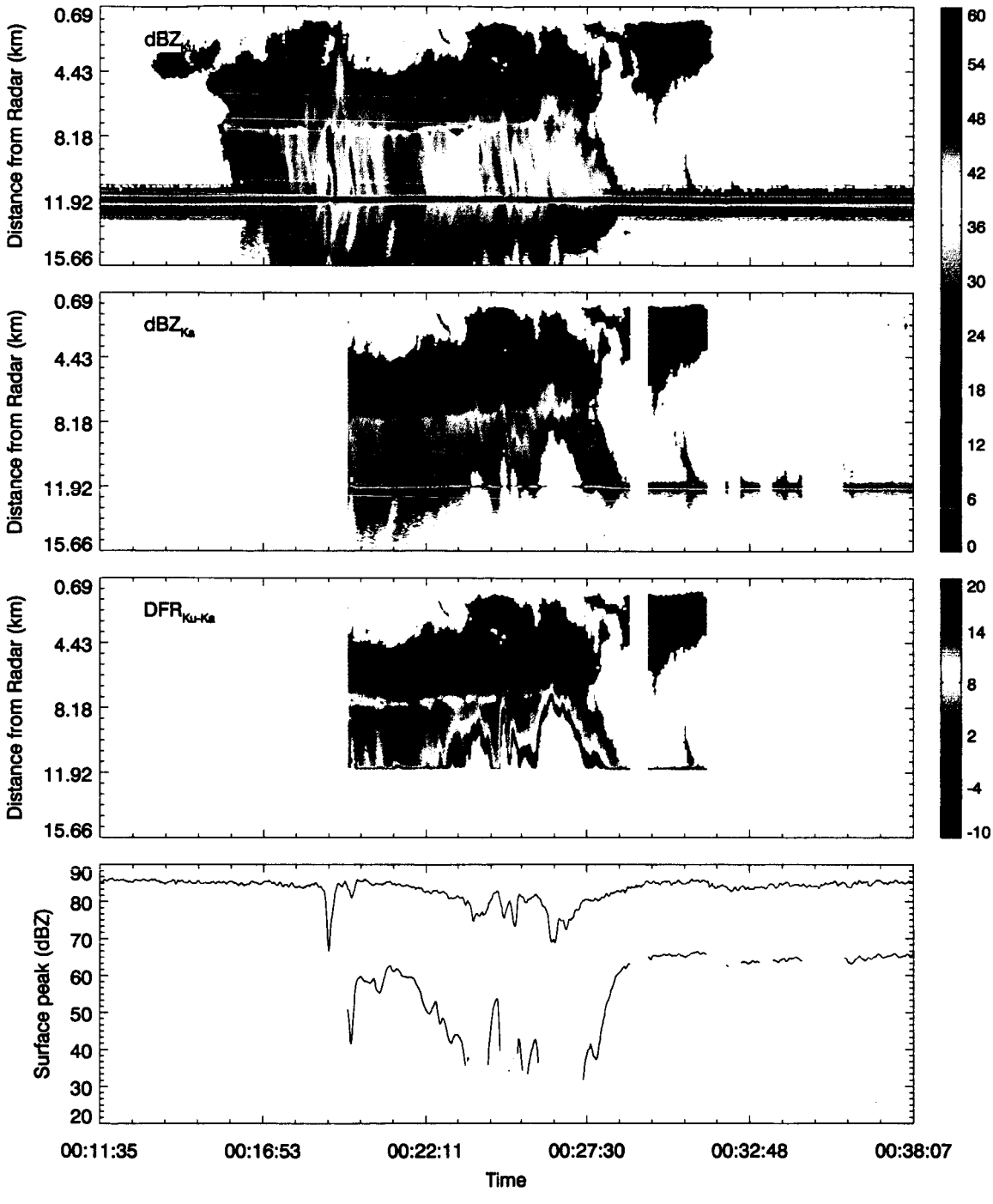

Fig.7 The PR-2 measurements over a rain cell taken on 25 September 2001 in Florida during the CAMEX-4. The surface powers are also plotted (bottom panel) with the upper curve denoting the Ku band and the lower the Ka band.

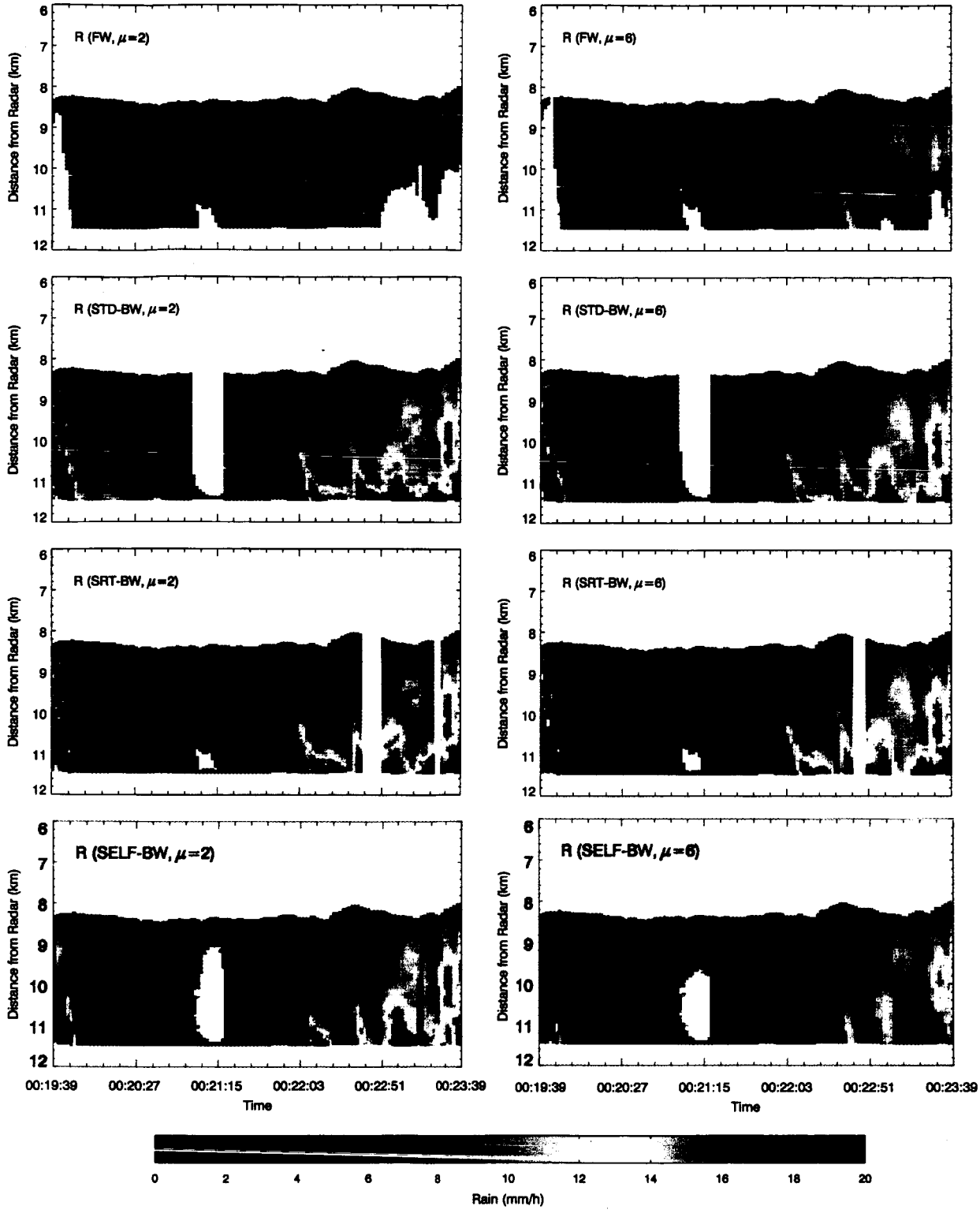

Fig.8 Estimates of rain rate from the PR-2 measurements shown in Fig.6 by use of forward, backward and self-consistent approaches as μ is assumed to 2 and 6.